Reversible Alignment of Nanoparticles and Intracellular Vesicles During Magnetic Hyperthermia Experiments

FERNÁNDEZ-AFONSO, Yilian, RUTA, Sergiu, PÁEZ-RODRÍGUEZ, Amira, VAN ZANTEN, Thomas S., GLEADHALL, Sian, FRATILA, Raluca M., MOROS, María, MORALES, Maria del Puerto, SATOH, Akira, CHANTRELL, Roy W., SERANTES, David and GUTIÉRREZ, Lucía

Published version

FERNÁNDEZ-AFONSO, Yilian, RUTA, Sergiu, PÁEZ-RODRÍGUEZ, Amira, VAN ZANTEN, Thomas S., GLEADHALL, Sian, FRATILA, Raluca M., MOROS, María, MORALES, Maria del Puerto, SATOH, Akira, CHANTRELL, Roy W., SERANTES, David and GUTIÉRREZ, Lucía (2024). Reversible Alignment of Nanoparticles and Intracellular Vesicles During Magnetic Hyperthermia Experiments. Advanced Functional Materials.

ADVANCED FUNCTIONAL MATERIALS
www.afm-journal.de

Reversible Alignment of Nanoparticles and Intracellular Vesicles During Magnetic Hyperthermia Experiments

Yilian Fernández-Afonso, Sergiu Ruta, Amira Páez-Rodríguez, Thomas S. van Zanten, Sian Gleadhall, Raluca M. Fratila, María Moros, Maria del Puerto Morales, Akira Satoh, Roy W. Chantrell, David Serantes, and Lucía Gutiérrez**

Heating magnetic nanoparticles (MNPs) with AC (Alternating Current) magnetic fields has received significant attention in recent years, particularly for biomedical uses. However, most studies focus on characterizing the heat release, overlooking the fact that the MNPs in the viscous cell environment constitute a dynamic magnetic colloid whose configuration may evolve over time, particularly if a driving force as the AC field is applied. Aiming to shed light on this matter, in this workthe dynamics of the colloid structure during hyperthermia experiments are studied. By combining various experimental and theoretical tools, it is concluded that the AC field may drive the formation of aligned structures, and the impact that such structures may have on the associated heating is assessed. Remarkably, the results show that those field-driven structures are highly unstable for small particle sizes, rapidly disassembling upon field removal. Moreover, an analogous behavior in vitro is found, with the AC magnetic field also promoting a reversible alignment of vesicles containing the MNPs within the cells. The results suggest that the observed alignment, both of MNPs and intracellular vesicles, may be a common phenomenon in usual hyperthermia experiments, but unnoticed because of the intrinsic unstable nature of the aligned structures.

1. Introduction

A huge amount of work has been made by the research community in the past two decades exploring the heating properties of magnetic nanoparticles (MNPs) when exposed to an alternating magnetic field. This effort is justified given that such heating properties are crucial for the subsequent application of the particles, mainly as part of cancer treatments by magnetic hyperthermia but also in novel interesting applications, such as organ warming after cryopreservation,[1] enzymatic reaction catalysis,[2] or remote manipulation of thermosensitive cellular channels.[3]

A common characteristic of such diverse applications is the requirement of very accurate doses of delivered heat, especially for biomedical applications, as over- or infra-heating could either cause damage or insufficient effect. Despite the advancements in the field of hyperthermia, interlaboratory studies focused on the measurement of the heating performance of magnetic nanoparticles revealed an important problem, namely the high variability of results between different research groups.[4] These measurements are usually performed in terms of the specific loss power (SLP) or the Specific Absorption Rate (SAR) (although this last term should be used solely to describe power dissipation in tissues).[4] Although a big effort has been recently made on the development of standard operating procedures,[5] there is still

Y. Fernández-Afonso, A. Páez-Rodríguez, T. S. van Zanten, R. M. Fratila, M. Moros, L. Gutiérrez
Instituto de Nanociencia y Materiales de Aragón (INMA, CSIC/UNIZAR) and CIBER-BBN
Zaragoza 50018, Spain
E-mail: lu@unizar.es

S. Ruta, S. Gleadhall
College of Business, Technology and Engineering
Sheffield Hallam University
Sheffield S1 1WB, UK

The ORCID identification number(s) for the author(s) of this article can be found under https://doi.org/10.1002/adfm.202405334

DOI: 10.1002/adfm.202405334

M. del P. Morales
Materials Science Institute of Madrid (ICMM/CSIC)
Madrid 28049, Spain

A. Satoh
Akita Prefectural University
Akita 010-0195, Japan

R. W. Chantrell
Department of Physics
University of York
York YO10 5DD, UK

D. Serantes
Applied Physics Department and Instituto de Materiais (iMATUS)
Universidade de Santiago de Compostela
Santiago de Compostela 15782, Spain
E-mail: david.serantes@usc.gal

no agreement on the measurement protocol or the data analysis procedure for the determination of SLP.[4]

Another important reason hindering the advancement of this research area is the complexity of the physical problem underlying such measurements.[6] In addition to the AC field conditions or the particle characteristics, there are other factors, often neglected, that may play a fundamental role in the heating properties of the magnetic colloids such as the interparticle dipolar interactions or the rotation capability depending on the media viscosity.[7] Lack of knowledge of such important variables may be the reason for the inconsistency of some of the reported results.

One aspect that has been poorly studied is the possible dynamic evolution of the magnetic colloid over time as a consequence of the exposure to the AC (alternating current) field, which may promote, for example, the organization of the particles into elongated assemblies or chains. However, while the formation of elongated aggregates has been widely reported for ferrofluids exposed to DC (direct current) magnetic fields,[8,9] or even not exposed to magnetic fields,[10] only a very limited number of works have focused on MNPs chain formation when exposed to AC magnetic fields.[11–15] Considering the crucial role of chaining on the heating performance,[16,17] we believe that this aspect has been significantly overlooked and deserves a more in-depth study. Since a change in the particle arrangement over time could lead to very different heating performances, the usual approach that a given MNP system is characterized by a single SLP value may not be correct.

As chain formation is a dynamic process, the time needed for the initial chain arrangement or the evolution of the length and thickness of the chains during the magnetic hyperthermia measurements may be critical parameters to consider in the understanding of the variability of experimental results. This is especially relevant, as pointed out by Mille et al.,[15] as most of the experimental methods to determine the SLP value of a suspension of MNPs rely on the analysis of the initial time points during the heating process. Indeed, the analysis of the initial slope of the temperature time dependence is used as a gold standard considering that, in non-adiabatic systems, the increase in temperature produces a linear response only over the initial time points.[18] Therefore, if chaining occurs, altering the heating properties over time and as a consequence causing a non-linear behavior, new approaches for the data analysis of the SLP would be required. Thus, the SLP value is no longer a constant that characterizes the heating of the system, but instead becomes time-dependent, i.e., $SLP = SLP(time)$.

Moreover, it should also be considered that the clinical use of magnetic hyperthermia for cancer treatment is being tested in animal models or in patients applying AC magnetic fields for lengths ranging mostly between 10 and 60 min.[19] Therefore, the impact that chain formation has on the heating properties of the particles during the treatment, or even the possible mechanical effects of chaining may have at the tissue, cell, or organelle level should not be overlooked. Indeed, previous works have pointed out the possibility of mechanical damage generation during AC magnetic field exposure in the frame of magnetic hyperthermia treatment, but it has been associated only with the use of cobalt-iron nanocubes,[20] or ferromagnetic microdiscs,[21] and has not been described for iron oxide nanoparticles, more typically investigated in the frame of in vivo studies[19] given their high biocompatibility properties.

The impact of the dynamic transformations that the chaining process over time has in very different applications is enormous, first because dynamic adjustments in the field conditions would be required for matching the required heat doses. Moreover, for the bio-related applications (not only cancer treatment, but also the other aforementioned ones, such as drug release,[22] magnetogenetics,[23] etc.) because if long chains are being formed in vivo, those might cause other effects beyond simply heating; for example, tissue damage, or opening of mechanically-activated ion channels if in their proximity. On the other hand, in other applications such as for example renewable energy storage[24] or catalysis,[2] a growing heat production over time with a lack of control may be detrimental for reproducibility issues. Thus, knowledge about the dynamic transformations occurring during the AC magnetic field exposure is needed urgently for the development of new applications making use of MNP-based heat production, or for improving the current ones.

However, tracking the chain formation in real time during the exposure of MNPs to AC magnetic fields has significant difficulties. Liquid suspensions are usually located inside the coil that generates the magnetic field, so the direct observation of the ferrofluid is limited. Moreover, chain lengths in the nanometre scale will not be observed directly in the suspension and high resolution characterization techniques, such as electron microscopy, that require removing the sample from the coil would be needed, thereby prohibiting the observation of the dynamical changes of the particle structures. As a consequence, the number of works on this topic is scarce. Saville et al. have observed chain formation by placing the particles into a resin that hardens during the exposure to the AC field and a subsequent observation by optical microscopy or magnetic characterisation of this single time point.[11] Nevertheless, this approach only allows a single time point analysis. Recently, other works have been able to track chain formation over time by magnetic measurements using $FeNi_x$ nanoparticles,[15] or magnetite particles.[14] This approach, based on magnetometry, is very powerful for tracking the physical evolution of the system through changes in the magnetic signal. However, its use to study the chain evolution once the field is switched off is more complicated. Therefore, other approaches are necessary to follow both the chain formation and rupture over time. The problems becomes even more challenging when analyzing the process in biological media, such as cells or tissues, instead of colloids. The disassembly of the chains may occur really fast, requiring some procedure to capture the structure when the cells are inside the coil being exposed to the AC magnetic field.

In this work, we have used colloids of iron oxide particles of different sizes (large and small, ≈26 and ≈13 nm in diameter, respectively) and various experimental set-ups to monitor the chain formation and evolution over time during magnetic hyperthermia experiments using digital microscopes and different coils (open and closed). Our results indicate that elongated structures aligned with the field are formed under the AC field for both MNP sizes. We propose that the fast disassembly of the structures formed is the reason why it is so complicated to observe these structures in the classical experiments, supporting

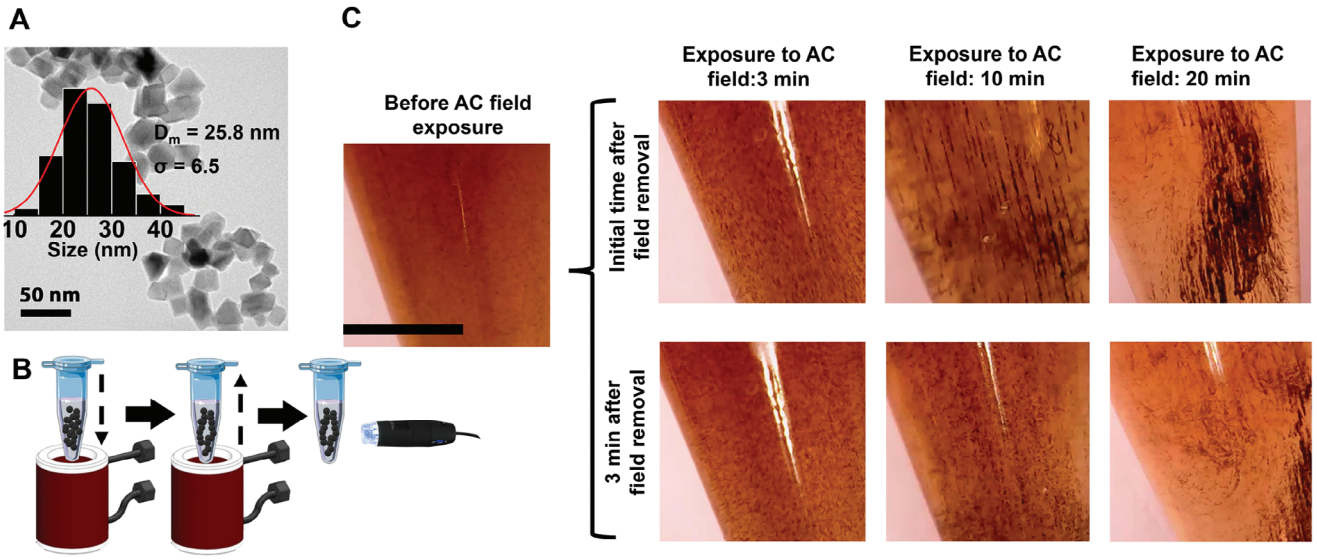

Figure 1. A) Transmission electron microscopy image and particle size distribution histogram for NPs-26. B) Schematic representation of the experiment to study the reversible alignment of MNPs exposed to AC magnetic fields. C) Photos of MNPs in resin immediately after the magnetic field was removed and three minutes later. Scale bar in the image corresponds to 0.5 cm. All images are at the same magnification.

the interpretation with computational results based on a newly developed code that combines colloid evolution (through Brownian dynamics) and magnetization orientation (through Monte Carlo simulations), to study the chain formation and disassembly. Moreover, we have also simulated the impact of chain formation on the heating properties of this type of particles. Finally, we have performed an in vitro test to verify if the elongated structures can be observed inside cells after the exposure to AC magnetic fields. Our results have shown that intracellular vesicles that contain the uptaken magnetic nanoparticles are aligned within the field during the AC magnetic field exposure.

Taken together, our results suggest that the formation of large structures aligned with the magnetic field are something common but rather unexplored in usual hyperthermia experiments. Nevertheless, more attention to the formation of such structures should be paid in the future, given the high impact that this dynamic evolution of the assemblies has on the heating properties of the particles.

2. Results and Discussion

We carried out an extensive investigation of the clustering process in magnetic nanoparticle systems and their potential effects on the heating process. Our combined approach of experimental and computational studies showed that field-induced chaining in a magnetic field (AC or DC) is reversible for small particle size, while for large particle size, the chaining is metastable: clustering persists but becomes less chain-like after the removal of the symmetry-breaking field. We also showed that in the cell environment, the nanoparticles are internalized by vesicles that themselves form chains in the presence of an AC magnetic field. We investigated theoretically the effects of the vesicle structures on the heat generation using a kinetic Monte Carlo model. For clarity, we separated the results into different sections.

2.1. Dynamic Nanoparticle Configuration: Spacial Ordering and Evolution in Magnetic Hyperthermia

We selected two types of iron oxide nanoparticles (≈26 and ≈13 nm in diameter) to track experimentally the formation of large structures that are aligned with the field direction during the exposure to an AC magnetic field. Different experimental approaches were needed to observe this behavior for each type of particle. The formation of larger aggregates by the ≈26 nm particles also allowed us to monitor the evolution of these structures once the AC field was removed.

2.1.1. Large Particles form Quasi-Stable Aligned Structures Under the AC Field

A first set of nanoparticles was selected to study the possible assembly processes occurring when the particles were exposed to AC magnetic fields. An oxidative precipitation method[25] rendering uncoated octahedral particles with a mean particle size, measured by the largest internal dimension of ≈26 nm (**Figure 1**A), was used for the synthesis. These particles were not coated and were denoted NPs-26.

As explained previously, one of the main difficulties of tracking the assembly of particles in colloids under the exposure of an AC magnetic field is that, as most coils used to apply the field are cylinders, the direct observation of the particle motion is limited. Moreover, the small size of the particles usually requires the resolution of electron microscopes for the possible assembly detection and therefore, a quick observation of the sample once it is removed from the magnetic field (inside the coil) is not straightforward. The NPs-26 were selected as their lack of coating makes them prone to a ggregate, which can be easily observed using a simple USB digital microscope located near the coil. This allows

a very fast capture of the images once the colloid is removed from the coil that applies the AC magnetic field.

Nanoparticles were placed in a EMbed-812 resin at 1 $mg_{Fe}mL^{-1}$. This resin has a viscosity of 4.1 cP at 25 °C,[26] that continuously increases during the hardening process as the temperature increases. This range of viscosity values was especially interesting as it was in the same range as lysosomes, the cell organelles where MNPs are usually located once they have been uptaken by the cells. In fact, a previous study by Hou et al. showed that the viscosity of lysosomes in MCF-7 tumor cells ranged between 9.04 to 94.8 cP.[27] Nevertheless, it must be kept in mind that the viscosity at the nanometer dimension is not an absolute parameter, as it depends on the dimensions of the particles embedded.[28]

The NPs-26 suspended in the EMbed-812 resin were placed inside the closed coil that applied the AC magnetic field (772 kHz, 360 Gauss) during three different times (3, 10, and 20 min) (Figure 1B). Images of the nanoparticles suspensions used for the magnetic hyperthermia experiments were collected just after AC field removal at the specified time points, and also 3 min after such field removal. Results indicated the formation of elongated structures aligned in the field direction whose length and thickness increased over time. Images acquired 3 min after field removal also showed the reversibility of these elogated structures, as they quickly started to break down into smaller - and not so aligned - aggregates once the field was switched off (Figure 1C). It has to be noted that the heat dissipated by the NPs- 26 was not enough to promote the resin solidification.

Previous work by Mille et al. showed that once these elongated structures were formed after the exposure to the AC magnetic field, they were stable for a long time and it was only possible to break these structures by sonication during several minutes.[15] However, in such case, the particles used for their study had a different size (of 17.3 nm) and composition ($FeNi_x$) than in our work, where the disruption of elongated structures occurs spontaneously in the resin once the AC magnetic field has been switched off. Other works that had studied dynamic changes in the formation of elongated structures occurring in colloids formed by iron oxide particles, were not able to evaluate their dynamics once the field was removed because of the limitations of the techniques used for the analysis.[11,14] Nevertheless, it is important to highlight here the work by Morales et al.[14] in which chain formation was reported in relatively similar particles (34 nm octahedrons) to the ones used here.

The resin used for these experiments was a viscous medium that may play a role on the dynamics of the MNPs alignment and disassembly, therefore a different set-up was used to follow this behavior in water suspensions, which are typically used during the characterization of the heating properties in SLP determination experiments. For these experiments an open and flat coil (PC90) was used (**Figure 2**A). This coil configuration allowed the direct observation of our glass container with the particle suspension during the magnetic hyperthermia experiments (147 kHz and 212 Gauss). A video of the experiment was recorded using two digital microscopes located on the top and lateral parts of the container (Figure 2A). In addition to using water as a suspension media, magnetic hyperthermia experiments were also performed both using the same resin described before for comparison (Figure 2B).

In these experiments, again, the formation of elongated structures was observed at the bottom of the container, next to the pancake coil. In fact, the size of the these structures increased over time, being more easily identified as the time of exposure to the AC magnetic field increased. This observation was clear from the images acquired from the lateral view of the sample holder. The formation of elongated structures ordered vertically resulted in a decrease of the aggregates observed from the top view. Once the field was switched off, the order of vertical chains started to disappear, observing a lower amount of chains in the bottom of the container from the lateral view and also an increase of randomly oriented structures from the upper view. Interestingly, the images acquired from the upper view at the initial time point and 2 min after field removal were slightly different, indicating that probably, within that time frame, chains were not completely destroyed, but instead they had misaligned. The low resolution of the images did not allow to perform any additional measurement regarding the chain length or thickness with appropriated accuracy. Nevertheless this procedure allowed tracking the dynamic transformation of the colloid in real time both while the magnetic field was ON but also when it was removed, a limitation observed in other characterization techniques that can only be used when the magnetic field is applied.[14]

These results indicated that the MNPs alignment observed in the resin in the experiments using the closed coil and the strongest AC magnetic field was reproduced using an open coil, a weaker magnetic field and different media. However, we wanted to assess if the observed behavior was related to the natural aggregation tendency of these uncoated MNPs. Therefore, a different procedure was used to test if the same phenomenon was also happening with smaller particles that were also more stable in the colloidal suspension.

2.1.2. Small Particles form Aligned Structures Under the AC Field, that Dissociate Upon Field Removal

Spherical (≈13 nm) iron oxide MNPs (**Figure 3**A) obtained by thermal decomposition in organic media and subsequently coated with PMAO (poly(maleic anhydride-alt-1-octadecene) were used (NPs-13-P) as an example of more stable colloidal suspension. These particles were prepared using the same synthetic and functionalization process that have been described in previous works.[29,30] Moreover, these particles were selected given the previous experience of the group using the same particles, that had been extensively used for in vivo biomedical applications, including the study of their long-term stability,[31] toxicity,[32] and efficacy in cancer treatment by magnetic hyperthermia.[33]

In order to avoid chain destruction after the AC field was switched off, particles were again placed in EMbed-812 resin. Another peculiarity of this resin is that it becomes solid above 60 °C, and because of that it is typically used in Transmission Electron Microscopy (TEM) embedding procedures, thus offering the possibility of solidifying our system during the magnetic hyperthermia experiments.

The particles were dispersed in the resin at 0.5 mg_{Fe} mL^{-1}. One microtube with 1 mL of this suspension was placed in our magnetic hyperthermia device (closed coil at 772 kHz and 360 Gauss) during 30 min and then transferred to a thermomixer at 60 °C

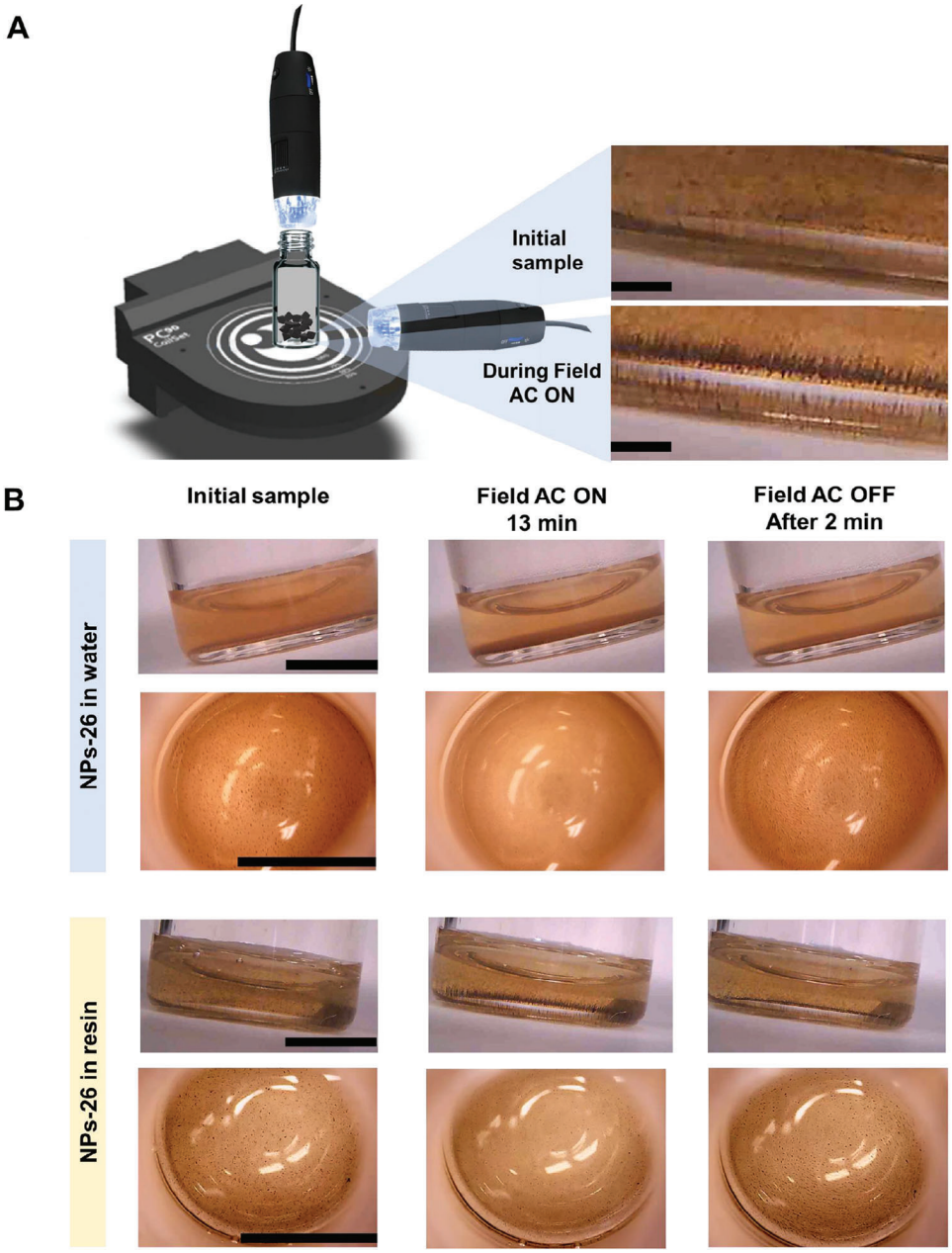

Figure 2. A) Schematic representation of the experiment for study of the MNP alignment when exposed to AC magnetic fields and disassembly upon field removal. Scale bar in the images corresponds to 0.1 cm. B) Photos of NPs-26 in water and resin before the AC field exposure, during the magnetic hyperthermia experiment (13 min with the AC field ON) and 2 min upon field removal. Scale bar in the images corresponds to 0.5 cm.

so that the resin fully polymerized (Figure 3B). The control microtube was placed in a thermomixer at 60 °C during the whole time. After that time, aggregates were observed by naked eye in the sample exposed to the AC field but not in the sample not exposed to the AC field. Sections of those solid samples were cut and observed by TEM. Interestingly, big and rounded aggregates were found in the sample not exposed to the AC field, while elongated structures were observed in the sample exposed to the AC field (Figure 3C). Although these experiments revealed the particle alignment during the AC magnetic field exposure, it was not possible to follow the evolution of these aligned structures over time and their subsequent dissociation upon field removal. The solidification procedure used in this work is not instantaneous and therefore there is a poor control on the time at which the elongated structures are being formed. Therefore, there is an urgent need to develop alternative characterization techniques that allow tracking these changes that may occur in very short time ranges.

These results, together with those from the previous section using the larger particles, prove the formation of elongated assemblies of nanoparticles when exposed to AC magnetic fields, at least with particles in the size range evaluated here and

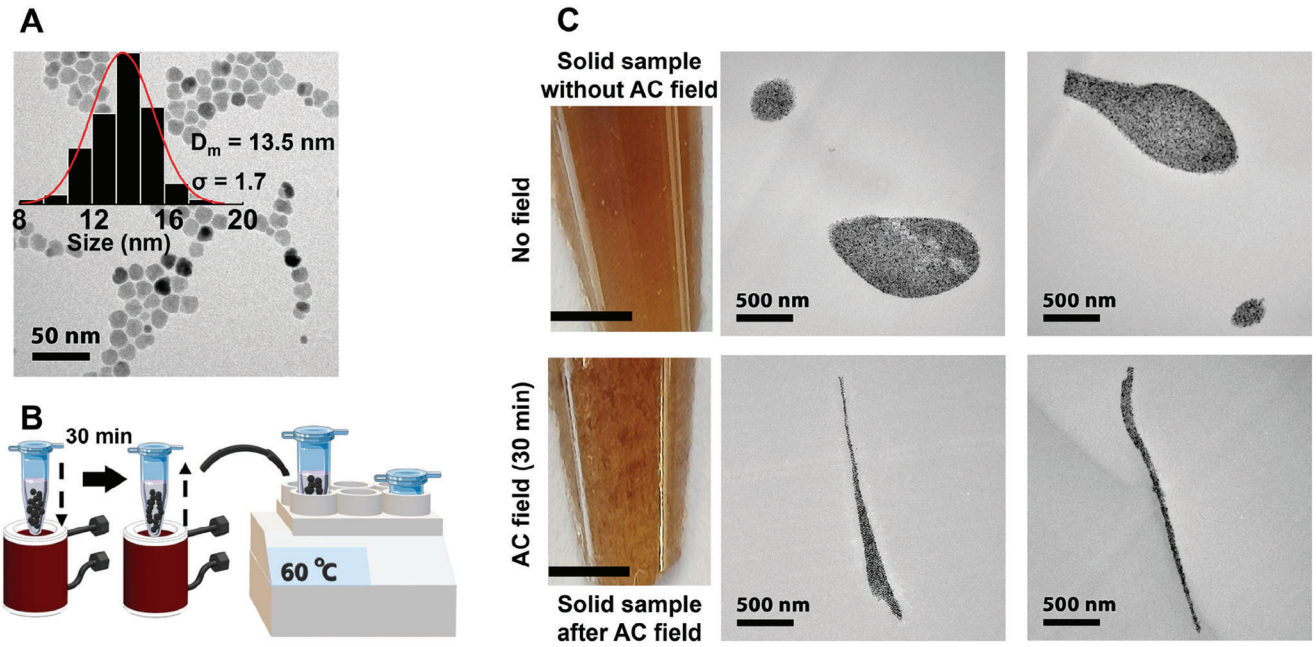

Figure 3. A) Transmission electron microscopy image and particle size distribution histogram for NPs-13-P. B) Schematic representation of the experiment to avoid chains destruction after the field was switched off. C) Images of the MNPs in resins either exposed or not exposed to the AC magnetic field. Scale bars in the images from the microtubes corresponds to 0.5 cm.

using the same AC magnetic field conditions. This phenomenon has been previously reported for iron oxide nanoparticle very few times in the literature,[11,14] however, it is still not clear if it will occur in all the AC magnetic field conditions or for iron oxide particles with slightly different properties (e.g., size, shape, coating, etc). Indeed, it is interesting to highlight here that the work by Morales et al.[14] tested particles with different sizes (12, 34, and 52 nm)[14] and showed that chain formation occurred only for the 34 nm particles but not for the other two sizes. Although the particle shape and AC field conditions were not the same as the ones tested here, we were able to observe chain formation in 13.5 nm particles. Therefore further work will be required to fully understand all the parameters (size, shape, AC field conditions, media viscosity, etc.) that may be playing an important role on the dynamic behavior of iron oxide particles exposed to AC magnetic fields.

These observations open a multitude of questions. In what follows, we have focused on exploring the following ones. First, why these aligned structures have not been described more often in the literature? Second, what is the time frame needed for such aligned structures to disassemble once the AC magnetic field is switched off? Third, what would be the impact of the alignment process on the heating properties of the material? And finally, will this process also occur inside cells?

2.2. Theoretical Insights Into the Evolution of Aligned Structures Once the Field is Off

Aligned structures of MNPs (referred hereafter as chains, for simplicity; but not necessarily single particle width chains) formed by the exposure to AC magnetic fields that subsequently remain stable -without a fixing agent- once the magnetic field is switched off have been described for compositions different from iron oxides.[15] Therefore, the scarce number of experimental observations of chain formation for iron oxide MNPs is probably related to the fast disassembly process occurring once the magnetic field is removed, as described in the previous section. In our experiments, we were only able to see the chains during the AC magnetic field exposure without a fixing procedure in the case of the bigger nanoparticles (NPs-26) in comparison to the smaller (NPs-13-P) where the chains were only observed if the resin was solidified to keep the structure stable. The results for the smaller particles clearly suggest the possibility that chains also exist for this size transiently (while the field is applied), but that they rapidly break down when the field is no longer applied. To study the role of the nanoparticle size on the disassembly process of the chains formed by iron oxide MNPs in water, complementary theoretical simulations were performed.

For the simulations we built a hybrid Brownian dynamics (BD) and Monte Carlo (MC) method that allowed us to consider both the evolution of the magnetic colloid, and of the inner-particle magnetisation. This was achieved by including within a well-tested BD code developed by A. Satoh,[34] the decoupling of the magnetization from the lattice in terms of a standard MC model for uniaxial-anisotropy particles.[35] The functioning of this implementation was tested in the thermodynamic limits for the relative orientation between particle direction (anisotropy axis) and moment orientation; see Experimental Section for a detailed description of the computational model.

Our model allows to consider the role of thermal fluctuations not only in the displacement and rotation processes, but also on the particle's magnetic moment orientation. This is to say,

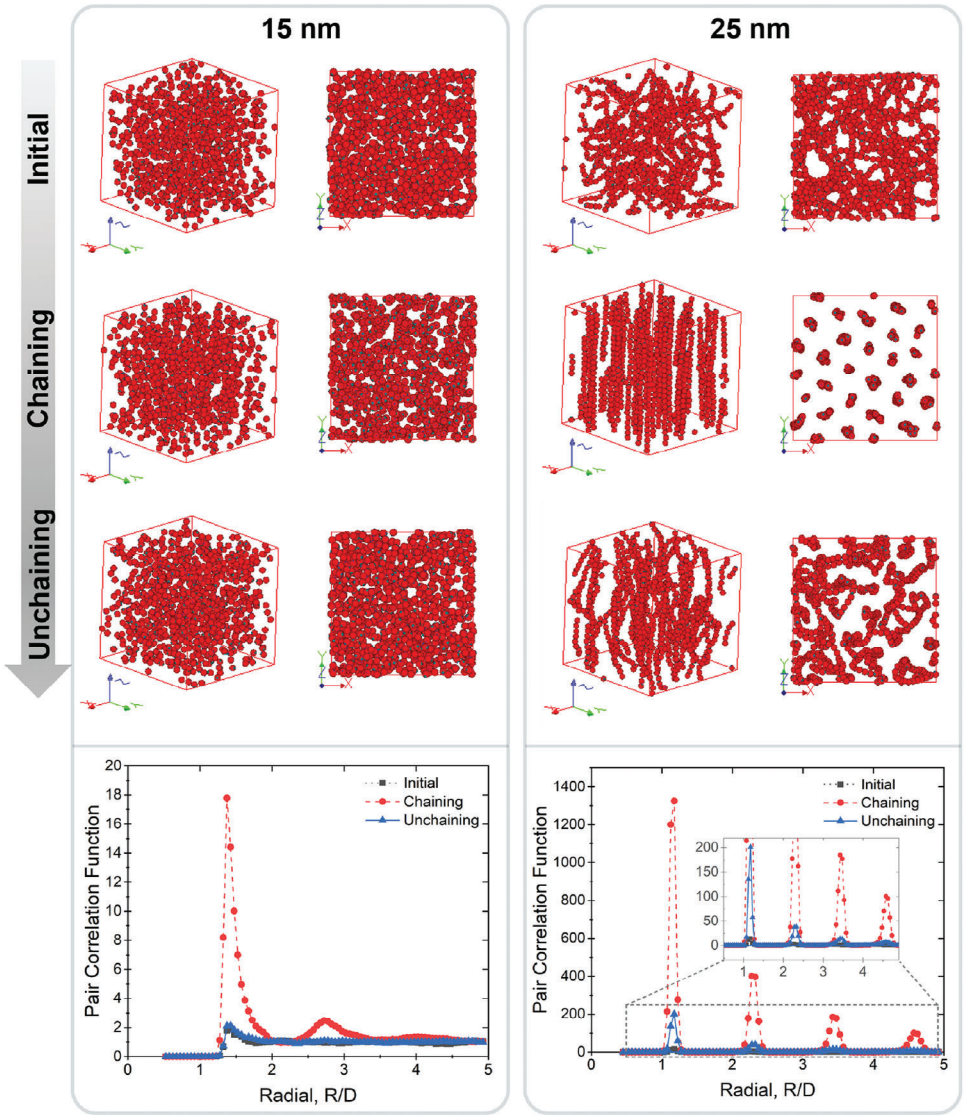

Figure 4. Spatial disposition of the simulated particle systems under different field conditions, for two different particle diameters: D = 15 nm (left panels), and D = 25 nm (right panels). For each size, two representative snapshots are shown for i) the starting (initial) configuration, ii) the field-driven one (chaining), and iii) the configuration after the field was switched off (unchaining). In each case, two views are shown: oblique -left-, and top -right- with respect to the field direction. The bottom graphs show the corresponding pair correlation functions of the different configuration stages.

we can go beyond the "magnetically blocked" assumption[36,37] to model the colloid evolution. Including such characteristics within the computational model is specially important for small particle sizes, as the particle magnetization reversal characteristic timescale (Néel time, τ_N) eventually becomes comparable -and then smaller- than the characteristic colloidal timescales of displacement (τ_d) and rotation (τ_B), therefore likely to have a significant influence on the colloid evolution.[38] This is the key objective of the simulations: to study the possibility of the chain formation in the case of small particles when subjected to an external field, and chain disassembly when the field is removed.

To study this scenario, we have simulated the behavior of magnetite particles in the range between 10 and 30 nm, in 5 nm intervals, from the initial configuration, under no field; then exposing the magnetic colloid to a strong DC magnetic field (chaining), and finally observing the system evolution when the field is switched off (unchaining). Note that, for computational efficiency, we are using a DC field to simulate the starting assembly structure of elongated aggregates. By doing so we can significantly speed up the simulations of this part, since under the strong DC field the magnetic moments of the particles are essentially aligned along the field direction[34,39] and the process of cluster formation is much faster than simulating the AC-field driven one. It is important to emphasise that such constitutes a very realistic assumption, as we have shown in the past that DC and AC fields lead to the formation of very similar structures.[40] Some representative snapshots of the simulation results for different field conditions are shown in **Figure 4**, for the sizes D = 15 and D = 25 nm, i.e., the ones closer to the experiments.

Analogous snapshots for the other sizes can be found in Figure S1 (Supporting Information).

Figure 4 shows the oblique and top (field direction) view of the sample particle positions for the different field stages simulated; see Experimental Section for details. Very different features were observed depending on the particle size: for the small size, a very random structure was observed for all three different stages (initial, chaining and unchaining); whereas for the large size, well defined chains were observed in all stages. Thus, for the $D = 25$ nm particles, even at the initial stage the presence of well-defined chains was observed, curved, and randomly oriented. Upon field application, the chains aligned along the field direction and reverted to more winding structure as the symmetry breaking field was switched off. We noted, however, that within the timescale of the simulation, the structure had not yet returned to its initial interpenetrating network structure. As a reference, we can highlight the much longer timescale explored for both the chaining and unchaining stages in comparison with the time needed to reach the initial random configuration. Thus, while the stationary initial stage is reached after two million iterations, for the chaining and unchaining steps the system was let to evolve for eight million timesteps in each case (see the Experimental Section for further details).

In a first approximation, therefore, it could be summarized that small sizes ($D = 10$ and 15 nm) do not form chains, and long ones ($D = 20$, 25, and 30 nm) always do. A closer inspection of the snapshots, though, revealed additional subtle features: for the $D = 15$ nm sample, at the chaining stage, it appeared to exist more empty space than in the other two stages. Comparing with the larger sizes, such bigger empty space could be an indication of chaining along the field direction. However, direct observation made it very difficult to raise any conclusion in this regard. Therefore, a complementary quantitative analysis was highly desirable to shed light on this matter and to this aim, we studied the pair correlation function (PCF).

The PCF, analogous to the usual radial distribution function (RDF), is a very sensitive parameter to characterize distributions of particles, providing information about the number of ambient particles stochastically distributed around an arbitrary particle, at an arbitrary radial distance. The difference is that while the RDF is evaluated in all directions, the PCF is evaluated around a certain direction, being therefore the ideal parameter to characterize the specific case of chains oriented along the field direction. Thus, while the chains could appear diluted when looking at the RDF (due to averaging along all angles), the PCF would clearly grasp the internal structure of the assembly.[41]

We, therefore, studied the PCF for each particle size, for the three field stages. The data, showed at the bottom of Figure 4, is a clear stamp that chains were transiently formed for the $D = 15$ nm size sample while the magnetic field was applied: a large peak (much larger than the initial stage one) was observed at the chaining state, but completely disappeared when the field was switched off. For the larger size, the presence of the high peaks for the three field stages indicated that chains were always present, as expected by observing the snapshots. The fact that the peak was much higher for the chaining stage was also in agreement with the observation of well-defined chains in the corresponding snapshots.

2.3. Impact of the Chaining Process on the Heating Properties of the Material

Previous theoretical[16] and experimental[42] results demonstrated that MNPs assembled into chains had different heating properties than the randomly assembled counterparts when exposed to AC magnetic fields. However, the impact of chaining may cause both a decrease or an increase of the particles heating properties, depending on the combination of particle properties and field conditions, as discussed by Valdes et al.[43,44] or Abenojar et al.[45] For example, in experimental approaches, Branquinho et al. found a decrease in SLP when increasing the chain length,[46] while Ranoo et al. found the opposite tendency.[47] In theoretical studies, Zubarev et al. found a decrease in SLP with increasing chain length,[48] while Anand et al. found an increase in SLP.[49] Another important aspect regarding chain formation was the possibility of chain reorientation under the field, depending on the viscosity of the environment,[17] as in addition to the change in hyperthermia performance -in that case also increase-, the physical rotation might in itself cause magneto-mechanical effects on the embedding media.

It is important to note here that, although new calorimetric approaches have been recently proposed,[50] the most widespread methods to determine SLP are generally based on the analysis of the initial temperature variation over the time generated when the particles are exposed to alternating magnetic fields. Therefore, changes in the local concentration or interactions among particles that may occur during the measurement, possibly due to chain formation, could lead to non-constant SLP values. This variability poses an important source of uncertainty in such measurements. In summary, it is unclear if dynamic chain formation plays a role in characterizing the heating properties of particles exposed to AC magnetic fields.

To evaluate the possible non-linear behavior of the SLP over time, simulations were performed to test the impact that chain formation had on the SLP values. SLP values were simulated for systems in which two different parameters were changed: the chain aspect-ratio (width/height) and the internal chain packing fraction. The calculation was based on the kMC model,[51] with model details provided in the Experimental Section. Based on the envisaged metastable field-driven chain formation above unravelled, this analysis was performed using the NPs-13-P particle size, as these smaller particles were drastically changing from a random distribution to forming aligned structures upon field application. Previous works have already evaluated the role of chain size on heating performance for larger particles, which may also reorient under the AC field.[17]

The experimental chains were generated within a cylindrical volume, maintaining the same chain width observed in the TEM measurements for the NPs-13-P (Figure 3). The aspect-ratio of the chains was varied for each packing fraction selected and the SLP values were calculated. It has to be noted that the local packing fraction of the chain structure was defined as the ratio of particle volume and the volume of the cylinder that encapsulated all the particles in a chain. Each chain contained particles with an average size of 13.5 nm with a standard deviation of 10% and random easy axis direction. For statistics, the calculation was repeated over several distinct chains such that the errors were less than the size of symbols used in **Figure 5**. For completeness, we

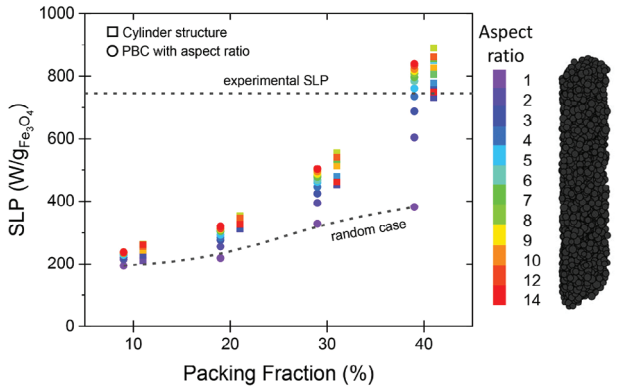

Figure 5. SLP calculated as a function of packing fraction and schematic representation of one of the elongated structures simulated. The color bar indicates the aspect ratio of the chain from 1 to 14. The cylinder structure (square symbols) was generated based on the width and height obtained from experimental configurations. Larger structures were generated using a periodic boundary condition and the effect of chain size was described using the aspect ratio of the chains. The results for cylindrical geometry were calculated using the same packing fraction as in the PBC case; however, the values were shifted to the right for ease of viewing. The simulation was performed with the same parameters as the experimental investigation: an AC field amplitude of 360 Gauss and a frequency of 772 kHz.

simulated indirectly very large chains using periodic boundary conditions, where the interactions were described by the local field of nearby particles, and the total demagnetization field calculated from the cylindrical geometry was given by the aspect ratio (see Experimental Section for details). For comparison, we also included the case of the aspect ratio of 1, which corresponds to the randomly dispersed particle for each packing fraction.

Results for the SLP values simulated for each of these conditions are plotted in Figure 5. A trend indicating that the increase in the packing fraction led to higher SLP values was clearly observed. However, when looking at the effect that chaining had on a specific packing fraction, interesting behaviors were observed. In particular, we found that for a small packing fraction, the actual relative orientation between particles played a minor role in the absolute SLP value, in other words, only slight differences in the SLP were found between aspect ratio = 1 and the rest of the chained structures. However, with increasing packing fractions the situation was dramatically different. Thus, for high local concentrations, changes in the aspect ratio different from 1 (corresponding to a random distribution) led to a much larger variation in the associated heating. As an example, when looking at the possible SLP values for the highest packing fraction, most of the SLP values of the elongated structures were in the range between 700 and 900 W $g^{-1}_{Fe_3O_4}$, compared to the 400 $^{-1}_{Fe_3O_4}$ of the randomly distributed structure. Taken together, all these results indicated that both the evolution of the chain length over time and the reduction in the interparticle distances may be having a combined effect on the heating properties of the system. Previous observations in theoretical simulations in which thinner chains (one particle width) were analyzed had also shown that the chain length was the crucial parameter affecting the SLP values.[17,40]

The SLP of these particles was measured experimentally (See Figure S2, Supporting Information) in the same AC magnetic field conditions using the closed coil described in the previous section and an iron concentration of 1 mg_{Fe} mL^{-1}, resulting in 744 ± 9 $Wg^{-1}_{Fe_3O_4}$. These results fall within the values obtained in the simulations for the highest packing fraction (40 %), indicating that during the measurement, magnetic nanoparticles were probably agglomerated and forming elongated structures. All these results suggested that the actual chain formation process is likely to play a significant role (bigger than reported thus far), to explain the differences observed in literature reports on SLP determination of the same material.

Additionally, these results could shed light on the variations in heating capacity among materials prepared with identical magnetic cores but different thicknesses of particle coatings, as in such cases, the use of thicker coatings could be hindering the attainment of higher packing fractions and therefore higher SLP values. Furthermore, these results confirm the observed tendency in which multi-core structures with particles in close contact usually display much higher SLP values than their single-core counterparts.[52]

Therefore, as a consequence of these observations, it will be fundamental to evaluate the time frame in which these chaining processes occur, especially in the frame of SLP calorimetric determinations and if this behavior is having an impact on the SLP calculation depending on the time analyzed for such characterization. These results may also highlight the interest in the new SLP characterization approach based on zig–zag measurements[50] as they will allow tracking SLP variations over time.

2.4. Alignment of Intracellular Vesicles Occurs in Cells

In the previous sections, we demonstrated the impact that chain formation in colloids has on basic characterization procedures widely used in magnetic hyperthermia experiments. However, it is important to note that these assembly processes have a very strong impact also on the applications in which MNPs are being used to produce local heat in biological environments (e.g., cells or tissues) when exposed to AC magnetic fields. Therefore, our objective was to evaluate assembly processes occurring in cells during the AC magnetic field exposure.

We chose a murine macrophage cell line for the test, as our previous experience with this cell line revealed high MNP uptake capacity of particles without signs of toxicity.[29,30] Indeed, using this same cell line and very similar nanoparticles, we were able to achieve iron concentrations (corresponding to the MNPs and not endogenous Fe) in the range between 1.2 and 7.5 pg_{Fe}/cell, also reaching a percentages of nanoparticle loaded cells above 90%.[29] Moreover, we functionalized the NP-13-P particles with a fluorophore (tetramethylrhodamine 5(6)-carboxamide, TAMRA) that allows tracking the particles by fluorescence microscopy and glucose (NP-13-PTG), that improves the particles stability and cellular uptake.[53] Cells were incubated with the particles for 1 h, washed and exposed to an AC magnetic field similar to the one used in Section 1 for the tests in water in the flat coil (148.5 kHz and 212 Gauss) but using the closed coil instead. These AC magnetic field conditions were selected so $H*f$ was $2.5*10^9$ Ams^{-1}, being below the biological limit proposed by Hergt et al ($5*10^9$ Ams^{-1}).[54] The AC magnetic field was applied for 20 min in all cases, except the control (cells incubated with MNPs, but not exposed to the magnetic field). In order to avoid the possible

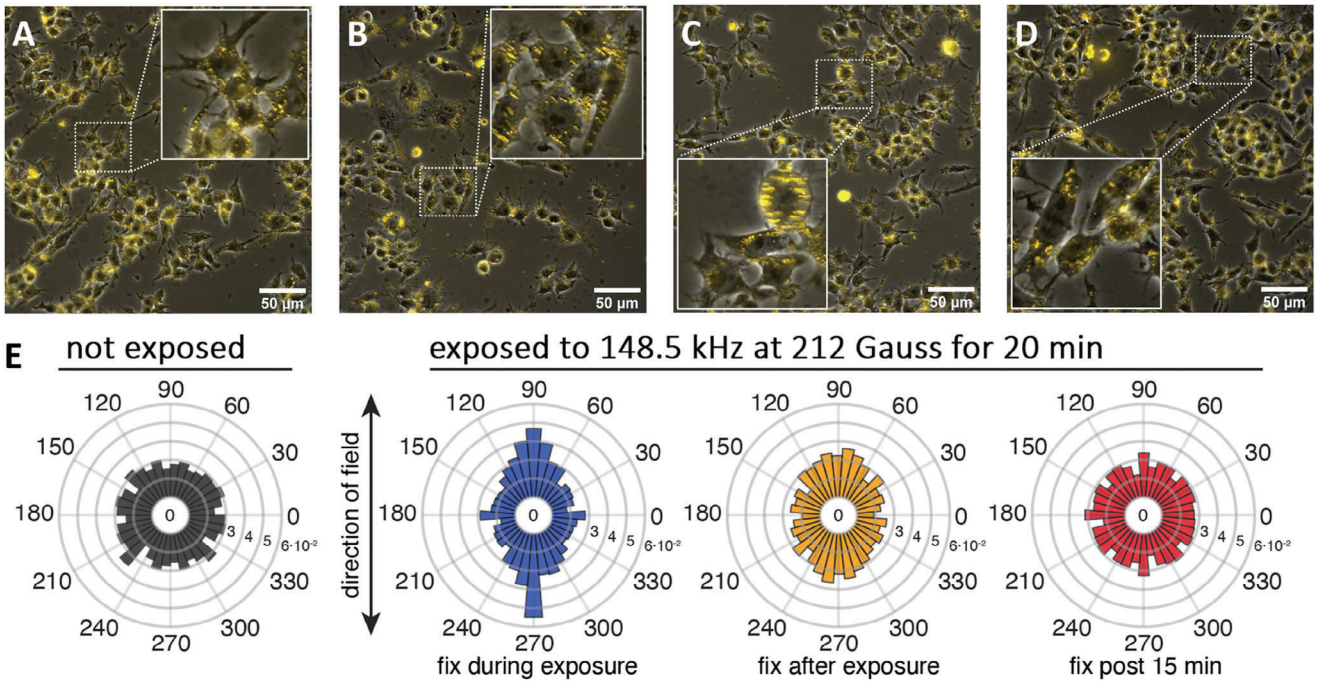

Figure 6. Optical microscopy images of the cell with MNPs A) no exposure to magnetic field, B) fixed during the exposure to magnetic field, C) fixed just after the exposure to magnetic field and D) fixed 15 min after the exposure to magnetic field. E) Quantification of the angle-distribution of nearby vesicles for the experimental conditions displayed in (A–D).

disassembly of the structures, a fixative was added to the cells to preserve their structure, at different time points: 1) 15 min after the AC magnetic field was switched on, so the fixation occurred during the last 5 min of field application; 2) immediately after the AC magnetic field was switched off and 3) 15 min after the magnetic field was switched off (See Figure S3, Supporting Information). While fixation with paraformaldehyde is standard procedure to preserve ultrastructural information for subsequent electron or fluorescence imaging, it is not instantaneous.[55] We therefore argued that the ideal condition to understand potential magnetic particle rearrangement in cells would be to fix during the application of the AC-field. The last 5 min of the AC-field application were selected as the fixation period so as to switch off the AC magnetic field once the cells were completely fixed. Subsequent optical microscopy images were acquired on the fixed cells exposed to the AC magnetic field and also on control cells that were not exposed to the field. The TAMRA fluorophore allowed the distinction of the particles location within the cells.

As expected, after treating the cells with MNPs for 1 h, we were able to detect their presence inside a multitude of randomly positioned vesicles that are likely associated with the general endosomal pathway[53] (**Figure 6A**). Strikingly, when these MNP-loaded cells were exposed to the AC magnetic field and fixed while the magnetic field was still on, those vesicles perfectly aligned in the field direction forming elongated structures (Figure 6B). These elongated structures were observed in the cytoplasm of the cells, but never surpassing the cell membrane limits or the nucleus membrane. This observation indicated that, while the cells were exposed to the AC magnetic field, movement of the intracellular vesicles occurred in order to achieve this configuration. However, during the 15 min of exposure without fixative the formation of such elongated structures did not visibly distort cell morphology. To quantitatively assess the local reorganisation of the vesicles, the relative angle distribution of all particles within a 1 µm radius were accumulated in a polar plot for each particle (see Experimental Section for details). Summing up the results from $>10^4$ particles clearly demonstrated the orientational bias of all the vesicles to align themselves to the AC magnetic field (Figure 6E). Experiments in which the fixative was added to the cells just after the exposure to the magnetic field (Figure 6C) and 15 min after the field was switched off (Figure 6D) shows a progressive relaxation back to the original random distribution (Figure 6E). This data not only demonstrated the quick disassembly of such structures with time but also revealed why similar findings have not been reported previously. Indeed, it is important to highlight that, as far as we know, this is the first time this behavior is being reported in the literature. Further work will be required in the future testing different AC magnetic field conditions, cell types or particle loading per cell to fully ellucidate all the parameters governing MNP assembly inside cells during magnetic field exposure.

These results open the way to a multitude of questions about the possible impact of the mechanical movement of the endosomes within the cells, and how the application of the AC magnetic field for different times or with bigger endosomes (for example as a consequence of a higher concentration of nanoparticle uptake) may affect the cell viability. Moreover, the fact that the intracellular vesicles seem to be interacting among them forming these long structures may also affect the heating properties of the material, as described in Section 2.3. Therefore, next, we succinctly explored such scenario.

By comparison of the fluorescence intensity with the individual particles adhered to the glass surface, an average value of

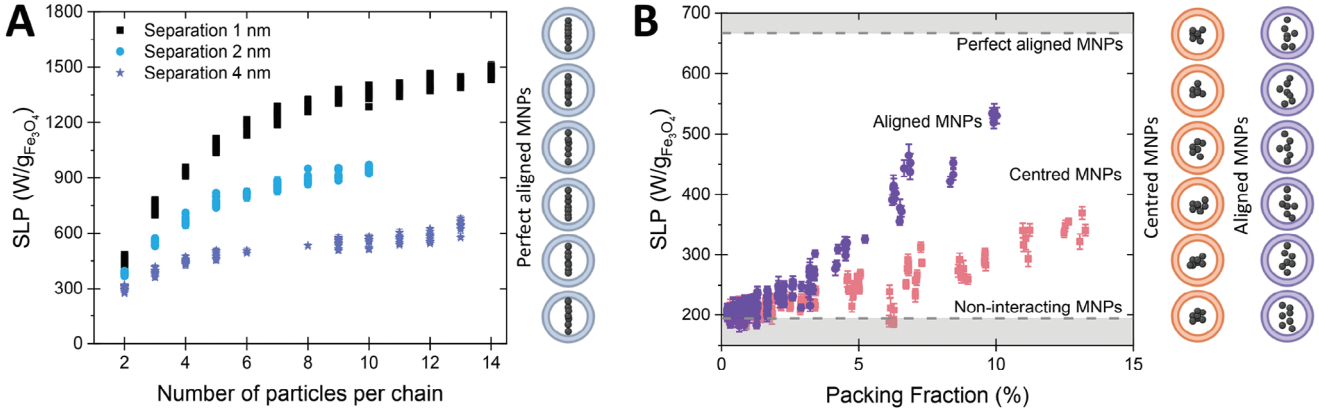

Figure 7. SLP values of different possible arrangements of MNPs within vesicles. A) MNPs were forming a perfect chain, where each particle was placed along the chain direction at a fixed separation (1, 2, or 4 nm) from the previous one. b) MNPs were generated inside the vesicle in two local configurations. First, a spherical cluster of particles was generated around the center of the vesicle, where the size of the sphere and the number of particles determine the local packing fraction. The second configuration was based on particles being placed in a cylinder geometry inside each vesicle, where the radius of the cylinder and the number of particles were varied to obtain different packing fractions.The simulation was performed with the same parameters as the experimental investigation: an AC field amplitude of 360 Gauss and a frequency of 772 kHz.

9 ± 5 nanoparticles per vesicle was obtained (see Experimental Section for additional details). Thus, considering this number and an average vesicle size of ≈100 – 500 nm, as reported by Klu et al.,[56] we theoretically constructed different particle distributions within the vesicles, and calculated the associated SLP value, as described in Section 2.3. Three possible cases were considered, in relation to the vesicle alignment direction: perfectly aligned MNPs (one particle width chains), aligned nanoparticles with some dispersion around the field axis, and centered nanoparticles (around the vesicle center). Schemes of the three cases are drawn in **Figure 7**. In all cases, the vesicles were aligned keeping a 30 nm distance between them.

First, a variable number of particles, between 2 and 14, was used to produce perfectly aligned chains (Figure 7A). This arrangement resembles the chains naturally occurring inside magnetotactic bacteria, which are also intensively investigated for hyperthermia.[57,58] Three different interparticle distances were evaluated (1, 2, and 4 nm). In this case, large variations of the SLP values were observed depending on the number of MNPs inside each vesicle. A fivefold increase in the SLP values was observed between the limits of weak interacting particles and more interacting particles. Differences in the SLP values depending on the number of MNPs were more pronounced in the case of the smallest interparticle distances.

For the other two spatial arrangements within the vesicles, a local packing fraction was used, constraining either the number of particles or the volume where the particles can be located inside each vesicle. The results are shown in Figure 7B. In both configurations, the SLP values increased with the packing fraction. Those values were always in the range between the non-interacting particle system and the values obtained for the perfectly aligned chains using the same interparticle distances. For the lower packing fractions (<3 %), no clear differences in the SLP values were detected among the different configurations.

The fluctuations in SLP values, that depend upon the MNPs local spatial arrangement highlight a significant challenge in the use of magnetic hyperthermia for therapeutic purposes. Without meticulous control over particle arrangements inside cells, regulating the heat dose administered to patients becomes unattainable. Hence, future works should prioritise resolving this lack of control.

3. Conclusion

We have shown that, during the magnetic hyperthermia experiments, the MNPs form elongated structures and that, consequently, this alignment will have a strong impact on the heat produced by the particles. This process is dynamic, as chain size increases with time. As a consequence, the SLP value generally used to characterize the heating properties of a material should no longer be assumed to be a constant, but instead it should be considered a time-dependent parameter. Further work is needed in order to get insight into the time scales in which these processes occur. This would be especially important for the definition of a standardized protocol for SLP determination to reduce inter-laboratory discrepancies in the future.

In addition, it has been proved that the assembly of iron oxide nanoparticles into chains is strongly size-dependent: whereas the elongated structures induced in large particle systems may still be observable once the field is switched off, a completely different behavior is observed in small size particles, which undergo a reversible process, as particles quickly disassemble upon field removal. Thus, for a given particle composition, the particle size is a key parameter governing the chain formation and subsequent disassembly. It will be the subject of a future work to study the role of the anisotropy in this general scenario.

In addition, another type of alignment has been observed in vitro, when cells loaded with MNPs are exposed to an AC magnetic field. In this case, intracellular vesicles containing the particles, align following the field direction. Although the first observations apparently indicate that this movement does not to disturb neither the cell nucleus nor the cell morphology, further studies are needed to assess if cells suffer any mechanical damage. The new spatial configuration of the vesicles generated by

the field may also have further consequences on the heating properties of the particles. Furthermore, our simulations suggest a strong role of the specific particle arrangement within the vesicles, therefore claiming for an in-depth further investigation to clarify the arrangement of the particles within the vesicles.

Summarizing, our results indicate that the usually accepted paradigm of a static MNPs arrangement assumed in the interpretation of magnetic hyperthermia experiments has a limited range of applicability. MNPs in a viscous medium may dynamically change their arrangement over time under the exposure to the AC magnetic field, and subsequently their heating properties. Moreover, the formation of the elongated structures could introduce additional ways of action into the entire field of magnetic hyperthermia, through magnetomechanical effects.

4. Experimental Section

Particle Synthesis and Characterization: Two synthetic approaches were used in this work. The first set of nanoparticles (≈26 nm) were synthesized by precipitation of an iron (II) salt ($FeSO_4$) in the presence of a base (NaOH) and a mild oxidant (KNO_3), following previously described synthetic protocols.[25] These particles were not coated (NPs-26). The second set of nanoparticles (≈13 nm) were synthesized by thermal decomposition of an iron acetylacetonate precursor in the presence of oleic acid following previously described protocols.[29] Nanoparticles were transferred to an aqueous medium using an amphiphilic polymer (PMAO, Poly(maleic anhydride-alt-1-octadecene)) coating (NPs-13-P), as previously optimized in this group.[59]

The nanoparticles size was determined through Transmission Electron Microscopy (TEM) observations in a Tecnai G2 TEM (FEI) operated at 200 kV. Samples were prepared by placing a drop of the diluted suspension onto a carbon coated grid and allowing it to dry at room temperature. Particle size was measured as the longest internal dimension of the particle, measuring over 100 particles to determine the particle size distribution.

Experimental Study of the MNPs Alignment when Exposed to AC Magnetic Fields: For the chain observation in colloids, nanoparticles were dispersed either in a resin (EMbed-812) that becomes solid above 60 °C, or in water.

A commercial equipment (D5 Series from nB nanoScale Biomagnetics) was used as the AC magnetic field source for the hyperthermia experiments. Two different coils were used: a G model closed coil made of single solenoid tube coil set and a PC90 open coil made of pancake multilayer litz wire coil sets. The experiments in the closed coil were performed using two different combinations of the frequency and AC field amplitude (772 kHz, 360 Gauss and 148.5 kHz, 212 Gauss) while an AC field amplitude of 212 Gauss and a frequency of 147 kHz was used in the experiments in the open coil.

Chain formation of the NPs-26 was observed by placing the particles in the resin and exposing the suspension to an AC field (772 kHz, 360 Gauss) in the closed coil during different times (3, 10, and 20 min). After such periods, the sample container was removed from the coil and images of the chains formed were acquired using the digital microscope immediately and also 3 min after field removal.

In addition, chain formation in the NPs-26 sample was followed by placing the particles either in water or in resin in a glass container that was placed on top of the open and flat coil (PC90) and exposed to the AC filed (147 kHz, 212 Gauss) during 13 min. Videos from such experiments were recorded using two digital USB microscopes (1000X Magnification). One microscope was located to obtain a view of the particles suspension from the top and the other one was located on one side, to obtain a lateral view of the sample container.

Chain formation by the NPs-13-P was performed by placing the resin with the particles inside the closed coil during 30 min and transferring the sample to an Eppendorf Thermomixer at 60 °C afterward, until full polymerisation of the resin. Chains formed in such procedure were observed by TEM microscopy under the same experimental conditions described above. The only difference was that for such observations, the EMBbed-812 resin was cut into 50 – 70 nm thick slices in the longitudinal direction of the AC field. As a control sample for this experiment, particles were dispersed in the resin and kept in the Eppendorf Thermomixer at 60 °C until full polymerization of the resin. Sections of such hardened resin were also cut and observed under the TEM as described before.

In Vitro Experiments: For the in vitro experiments, the 13 nm nanoparticles surface was slightly modified during the transference to water process following previously described protocols.[30] PMAO was modified with TAMRA (tetramethylrhodamine 5(6)-carboxamide) cadaverine (Anaspec, Seraing, Belgium)), a fluorophore that allows tracking the particles inside the cells. Additionally, the coated particles were also functionalized with glucose (4-aminophenyl β-D-glucopyraniside), as this molecule provides better stability in cell culture media and improves the nanoparticle uptake by the cells. The resulting particles were named NPs-13-PTG (PMAO-TAMRA-GLUCOSE). The cell line selected for the experiments was the murine macrophage RAW-264.7. Cells were cultured and maintained in DMEM supplemented with 10% fetal bovine serum, 1% glutaMAX and 1% antibiotic (Penicillin Streptomycin) (cDMEM). Cells were seeded at a density of 300 000 cells per well onto 25 -mm diameter glass coverslips inside standard 6-well plates in 3 mL of supplemented DMEM and grown for 24 h under standard culture conditions. After that time, the cDMEM was removed and the cells were washed with M1 (20 mM Hepes, 150 mM NaCl, 5 mM KCl, 1 mM $CaCl_2$, 1 mM $MgCl_2$ and 2 mg mL^{-1} D-glucose at pH = 7.4) medium, and finally incubated with 150 μg_{Fe} (at 100 μg_{Fe} mL^{-1}) of the NPs-13-PTG in M1 during 1 h. After that, cells were washed with M1 to remove non-internalized particles and kept in that medium for the AC field exposure experiments at room temperature. Each slide was placed vertically inside in the closed coil (See Figure S3A, Supporting Information). Cells were exposed to an AC magnetic field (148.5 kHz, 212 Gauss) for a total of 20 min. Subsequently, in order to fix the cells at different times, a concentrated fixative (paraformaldehyde) was added to medium to achieve a 4% final concentration. The paraformaldehyde was added at four different time points: without AC magnetic field (control), after 15 min of magnetic field exposure, at 20 min of magnetic field exposure (when the AC field was turned off) and after 15 min of turning off the magnetic field (see Figure S3B, Supporting Information). Fixed cells were imaged on an Andor Sona sCMOS camera using a Nikon TiE equipped with a 40X-0.75NA (large field of view images) or 60X-1.4NA (orientation quantification) phase objective which with a 1.5X tube lens resulted in a pixel size of 163 and 72 nm, respectively. Vesicles filled with MNPs were readily visible using phase contrast but using fluorescence allowed us to quantify both the amount of nanoparticles per vesicle and the position of each vesicle. The TAMRA fluorophore was excited using a halogen lamp utilizing excitation filter (528 – 553 nm), a dichroic (565 LP), and an emission filter (577 – 630 nm) that separates excitation from emission. A power of 17 mWatt was used, the camera integration time was set at 100 ms and z-stacks of 5 – 12 µm were obtained at 300 nm axial slices. It was possible to clearly distinguish non-specifically adhered individual nanoparticles on the glass substrate and compare their intensity distribution with the intensities of vesicle in the cell. It was calculated that each of the 50 – 100 vesicles per cell will contain 9 ± 5 nanoparticles (see Figure S4A, Supporting Information). To identify vesicle positions imageJ was used to performed a maximum projection of the first 3 µm above the coverslide (see Figure S4B, Supporting Information) followed by a fast Fourier transform bandpass filter (see Figure S4C, Supporting Information) to get rid of out-of-focus fluorescence. Individual vesicles were clearly identifiable using the peak-find algorithm from imageJ. Next, for each vesicle its position (x_0, y_0) was determined as well as the (x_i, y_i) positions from all neighboring vesicles within a 1 µm radius (see Figure S4D, Supporting Information). The orientation of the line connecting (x_0, y_0) with (x_i, y_i) was determined via angle $= cos(\frac{\Delta x}{\sqrt{\Delta x^2+\Delta y^2}})$ in the case of $\Delta y < 0$, angle = 360 −angle. Finally, the angular data was binned in 10°-bins and the factional distribution of angles (see Figure S4D, Supporting Information) was summed up for >10000 vesicles to yield each of the polar plots of (see Figure 6).

Computational Models—: *Colloidal Model of Chaining*

Computational investigations of the colloidal structures was carried out using a hybrid model comprising a Monte-Carlo approach to the simulation of the interaction between the magnetic moment and applied field and Brownian Dynamics simulations of the translational and rotational degrees of freedom. This differs from previous approaches,[60–63] which concentrate on the rotational degrees of freedom. The nanoparticles were assumed to interact via a dipolar magnetostatic field and steric repulsion arising from the overlap of surfactant layers. The local dipolar field is the sum over pairs of particles *i* and *j* given by:

$$\vec{H}_i^{\mathrm{dip}} = \frac{1}{4\pi} \sum_{i \neq j} V_j M_s r_{ij}^{-3} \left(-\hat{m}_j + 3\hat{r}_{ij}(\hat{m}_j \cdot \hat{r}_{ij})\right) \tag{1}$$

where $\vec{r}_{ij} = r_{ij}\hat{r}_{ij}$ is the inter-particle distance. The volumetric packing fraction of particles is $\epsilon = N\langle V_i \rangle / V_s = NV/V_s$ and the average interparticle distance is $l = (V_s/N)^{1/3}$. For computational efficiency the calculation is carried out within a cut-off sphere of radius $r_c = 5.0D$, i.e., five times the particle diameter. The repulsive potential due to the overlap of surfactant layers is that given by Rosensweig et. al.,[64]

$$E^S = \frac{\pi n_s D^2 k_B T}{2} \left[2 - \frac{r_{ij}}{\delta} \ln\left(\frac{D + 2\delta}{r_{ij}}\right) - \frac{r_{ij} - D}{\delta}\right] \tag{2}$$

where D is the particle diameter, δ is the thickness of the surfactant layer and n_s is the surface density of the surfactant molecules. The magnetic behavior was calculated using a standard Metropolis Monte- Carlo approach.[65] The model also includes rotational and translational degrees of freedom to simulate the orientation of easy axes and the dynamical chaining process itself. This was done using calculated torques and forces in equations of motion given in ref. [66–68].

For the simulations, a size-monodisperse system of $N = 1000$ particles was employed. Periodic boundary conditions were considered both regarding particle positions and interparticle interactions, in a cubic box at a 3% volume fraction. The simulations assumed the macrospin approximation, i.e., coherent behavior of the inner atomic moments, so that the magnetic response of the particle is defined by its magnetic supermoment $\vec{\mu} = M_S V \hat{n}$, where M_S is the saturation magnetisation, V the particle volume and $\hat{n}$ the unit vector that described the magnetization direction. The anisotropy energy was taken as uniaxial, i.e., $E_A^i = -KVcos^2(\theta)$. Magnetite-like characteristics were assumed, using $M_S = 480kAm^{-1}$, and $K = 10^4 Jm^{-3}$. For the simulation runs, in each timestep, in addition to the rotation and displacement characteristic of the BD simulations, five random MC trial attempts for the magnetisation orientation were carried out, plus an additional Ising-like attempt of full magnetization reversal. The integration timestep size for the BD part was in all cases taken as $h = 0.000002$, and the MC attempts were within a standard 0.1 cone angle for the first five random ones, followed by the additional full-reversal one. No real time was considered.

To reach the initial configuration, the particles were first arranged in a simple cubic lattice, with the easy axes and magnetic moments oriented at random. Then, the three different systems arrangements reported in Figure 4 were simulated: first, the system was allowed to evolve freely - under no applied field- for two million timesteps (top "Initial" snapshots case); then, the system was subjected to an external DC field, of 2*T*, for over eight million timesteps (middle "Chaining" situation); finally, the system was let to evolve freely for other eight million additional timesteps (bottom "Unchaining" case). It was important to mention here that in all three cases the amount of simulation timesteps was chosen so that the system reached a stationary state, as evaluated through the evolution of the system magnetostatic energy (see Figure S5, Supporting Information)

In all cases, the particles were coated with a nonmagnetic layer of 3 nm thickness, i.e., $\delta = 3$ nm in Equation (2). Worthy to note, regarding the steric term, the simulations were in all cases conducted considering a constant ratio of steric interaction strength relative to the thermal motion, so that $\lambda_V = \pi D^2 n_s/2$ was constant for all cases; this value, taken as $\lambda_V = 150$ in base of previous works, implies in practice the same value of surface coating molecules (1200) for all particle sizes, from the $D = 30$ nm particles down to the 10 nm ones. It would be the subject of a further work to investigate the role of this dependence in detail.

To characterize the degree of chaining during the field-on/field-off sequence a pair correlation function (PCF), $g^{(2)}(\mathbf{r})$ was employed, that measures the local number density of particles along the field direction. Considering *z* the field direction in usual spherical polar coordinates, the number of particles could be denoted by $\Delta N_i(r, \theta, \varphi)$, located in the infinitesimal volume $\Delta V = r^2 sin\theta \Delta r \Delta\theta \Delta\varphi$ of the range $(r, \theta, \varphi) \sim (r + \Delta r, \theta + \Delta\theta, \varphi + \Delta\varphi)$ with respect to the i^{th} particle. Then, defining $n_0 = N/V$ as the number density for a uniform distribution of particles, where N is the total number of simulated particles and *V* the volume of the simulation region, the general PCF is defined as

$$g^{(2)}(\mathbf{r}) = \frac{1}{n_0} \cdot \left\langle \frac{1}{N} \sum_{i=1}^{N} \frac{\Delta N_i(r, \theta, \varphi)}{\Delta V} \right\rangle \tag{3}$$

Here, because of the chain-like symmetry induced by the magnetic field, the $\theta = 0$ was plotted, that was the PCF along the field direction $g^{(2)}(r)$.

Note that if the particles were uniformly distributed in the system the local number density was equal to n_0, so that $g^{(2)}(r)$ must be unity except in the case of particle chaining. To obtain the results shown in Figure 4, the intervals $\Delta r = 0.05D$, and $\Delta\theta = \Delta\varphi = 10\pi/180$ was used.

SLP Calculation by Kinetic Monte-Carlo

The SLP calculations were done using the kinetic Monte-Carlo (kMC) method The kinetic Monte-Carlo (kMC) method (see ref. [51] for more details) systematically incorporates the complexity of realistic particle distributions, thermal fluctuations, and time-varying external fields. In the present work, the uni-axial anisotropy $\vec{k}_i = K_i \hat{k}_i$, particle diameter D_i, and particle positions were randomized. The importance of interactions was controlled by adjusting the particle packing fraction ϵ for each chain structure with $\epsilon = 0$ implying the non-interacting case. The system energy is:

$$E = \sum_i \left(-K_i V_i (\hat{k}_i \cdot \hat{m}_i)^2 - \mu_0 V_i M_s \hat{m}_i \cdot (\vec{H} + \vec{H}^{eff}_{magnetostatic,i})\right) \tag{4}$$

with V_i being the volume of a particle *i*, M_s the saturation magnetization, $\hat{m}_i$ the particle moment normalised to unity and $\hat{k}_i$ is the particle easy axis direction as unit vector.

In the case of larger chain structure simulated using PBC, the interaction field was expressed as the sum of the dipole interaction field of all the particles inside a sphere of radius R_c, the demagnetisation field and the Lorentz cavity field. The effective magnetostatic field is:

$$\vec{H}^{eff}_{magnetostatic,i} = +\vec{H}_{dem} + \vec{H}_L + \vec{H}_i^{dip} \tag{5}$$

where H_{dem} is the demagnetization field given by the aspect ratio of the shape of the chain structure. The approximation for the demagnetization field for an ellipsoid of revolution with the same aspect ratio as for the chain structure was used. As the results indicate that in this case the size of the chain and the aspect ratio had a secondary effect on SLP, a more accurate method for describing the demagnetization factor for the chain structure was not needed. H_L and the Lorentz cavity field H_{dip} is the dipole field generated by the particles inside the cavity which is calculated using Equation (1).

It was important to mention that for the results reported in Figure 7A the particle size was generated with a 10% standard deviation from the mean value of 13.5 nm, and the number of particles per chain represented an average value over multiple chain structures. The chain structure was repeated such that the error bars were small. Regarding Figure 7B, the SLP values obtained in the two configurations were simulated using a variable number of particles between 10 and 50, in order to generate different packing fractions inside the vesicle (up to 15%).

Supporting Information

Supporting Information is available from the Wiley Online Library or from the author.

Acknowledgements

Authors would like to acknowledged financial support from the following projects: Project PID2021-122508NB-I00 funded by MICIU/AEI /10.13039/501100011033 and FEDER, UE; Projects PID2019-109514RJ-100 and PID2020-13480RB-I00 funded by MICIU/AEI /10.13039/501100011033; and Project CNS2023-144321 funded by MICIU/AEI/10.13039/501100011033 and NextGenerationEU/PRTR. Xunta de Galicia was acknowledged for projects ED431F 2022/05 and ED431B 2023/055. AEI was also acknowledged for the *Ramón y Cajal* grant RYC2020-029822-I to D.S. Funding from the European Research Council (ERC) under the European Union's Horizon 2020 research and innovation programme (grant agreement No 853468) was also acknowledged. Funding was also received from the European Commission through the TBMED project (DT-NMBP-02-2018, ID: 814439 to R.M.F.). In addition, the authors acknowledged the Centro de Supercomputacion de Galicia (CESGA) for computational resources. TSvZ was supported by a fellowship from the Fundación General CSIC's ComFuturo programme which had received funding from the European Union's Horizon 2020 research and innovation programme under the Marie Skłodowska-Curie grant agreement No. 101034263. The authors would like to acknowledge Fondo Social del Gobierno de Aragón (grupo DGA E15-23R), the use of Advanced Microscopy Laboratory (Universidad de Zaragoza), for access to their instrumentation and expertise. SR would like to acknowledge the Sheffield Hallam University Beowulf Cluster for computational resources. Last but not least, the profound impact of The Viking's contributions to this work cannot be overstated, as his expertise and dedication had been integral to its success.

Conflict of Interest

The authors declare no conflict of interest.

Data Availability Statement

The data that support the findings of this study are available from the corresponding author upon reasonable request.

Keywords

assembly, brownian dynamics, colloids, in vitro, kinetic monte-carlo, magnetic nanoparticles

Received: March 27, 2024
Revised: May 19, 2024
Published online:

[1] A. Chiu-Lam, E. Staples, C. J. Pepine, C. Rinaldi, *Sci. Adv.* **2021**, *7*, eabe3005.
[2] J. G. Ovejero, I. Armenia, D. Serantes, S. Veintemillas-Verdaguer, N. Zeballos, F. López-Gallego, C. Grüttner, J. M. de la Fuente, M. d. Puerto Morales, V. Grazu, *Nano Lett.* **2021**, *21*, 7213.
[3] S. del Sol Fernández, P. Martínez-Vicente, P. Gomollon-Zueco, C. Castro-Hinojosa, L. Gutierrez, R. M. Fratila, M. Moros, *Nanoscale* **2022**, *14*, 2091.
[4] J. Wells, D. Ortega, U. Steinhoff, S. Dutz, E. Garaio, O. Sandre, E. Natividad, M. M. Cruz, F. Brero, P. Southern, Q. A. Pankhurst, S. Spassov, *Int. J. Hyperthermia.* **2021**, *38*, 447.
[5] I. Rubia-Rodríguez, A. Santana-Otero, S. Spassov, E. Tombácz, C. Johansson, P. De La Presa, F. J. Teran, M. del Puerto Morales, S. Veintemillas-Verdaguer, N. T. Thanh, M. O. Besenhard, C. Wilhelm, F. Gazeau, Q. Harmer, E. Mayes, B. B. Manshian, S. J. Soenen, Y. Gu, Á. Millán, E. K. Efthimiadou, *Materials* **2021**, *14*, 706.
[6] P. Schier, C. Barton, S. Spassov, C. Johansson, D. Baumgarten, O. Kazakova, P. Southern, Q. Pankhurst, M. Coisson, C. Grüttner, A. Price, R. Rüttinger, F. Wiekhorst, J. Wells, U. Steinhoff, in *Polish Conference on Biocybernetics and Biomedical Engineering*, Springer, Berlin, Heidelberg, **2019**, pp. 316–326.
[7] D. Cabrera, J. Camarero, D. Ortega, F. J. Teran, *J. Nanopart. Res.* **2015**, *17*, 121.
[8] S. L. Saville, R. C. Woodward, M. J. House, A. Tokarev, J. Hammers, B. Qi, J. Shaw, M. Saunders, R. R. Varsani, T. G. St Pierre, O. T. Mefford, *Nanoscale* **2013**, *5*, 2152.
[9] N. I. Taib, R. C. Woodward, T. G. S. Pierre, K. S. Iyer, *IEEE Trans. Magn.* **2021**, *8*, 1.
[10] M. P. Arciniegas, A. Castelli, R. Brescia, D. Serantes, S. Ruta, O. Hovorka, A. Satoh, R. Chantrell, T. Pellegrino, *Small* **2020**, *16*, 1907419.
[11] S. L. Saville, B. Qi, J. Baker, R. Stone, R. E. Camley, K. L. Livesey, L. Ye, T. M. Crawford, O. T. Mefford, *J. Colloid Interface Sci.* **2014**, *424*, 141.
[12] I. Morales, R. Costo, N. Mille, G. B. Da Silva, J. Carrey, A. Hernando, P. De la Presa, *Nanomaterials* **2018**, *8*, 970.
[13] J. M. Asensio, J. Marbaix, N. Mille, L.-M. Lacroix, K. Soulantica, P.-F. Fazzini, J. Carrey, B. Chaudret, *Nanoscale* **2019**, *11*, 5402.
[14] I. Morales, R. Costo, N. Mille, J. Carrey, A. Hernando, P. de la Presa, *Nanoscale Adv.* **2021**, *3*, 5801.
[15] N. Mille, D. De Masi, S. Faure, J. Asensio, B. Chaudret, J. Carrey, *Appl. Phys. Lett.* **2021**, *119*, 022407.
[16] C. Martinez-Boubeta, K. Simeonidis, A. Makridis, M. Angelakeris, O. Iglesias, P. Guardia, A. Cabot, L. Yedra, S. Estradé, F. Peiró, Z. Saghi, P. A. Midgley, I. Conde-Leborán, D. Serantes, D. Baldomir, *Sci. Rep.* **2013**, *3*, 1.
[17] D. Serantes, K. Simeonidis, M. Angelakeris, O. Chubykalo-Fesenko, M. Marciello, M. D. P. Morales, D. Baldomir, C. Martinez-Boubeta, *J. Phys. Chem. C* **2014**, *118*, 5927.
[18] R. R. Wildeboer, P. Southern, Q. A. Pankhurst, *J. Phys. D: Appl. Phys.* **2014**, *47*, 495003.
[19] L. Beola, L. Gutiérrez, V. Grazú, L. Asín, in *Nanomaterials for magnetic and optical hyperthermia applications*, Elsevier, Amsterdam **2019**, pp. 317–337.
[20] P. B. Balakrishnan, N. Silvestri, T. Fernandez-Cabada, F. Marinaro, S. Fernandes, S. Fiorito, M. Miscuglio, D. Serantes, S. Ruta, K. Livesey, O. Hovorka, R. Chantrell, T. Pellegrino, *Adv. Mater.* **2020**, *32*, 2003712.
[21] D.-H. Kim, E. A. Rozhkova, I. V. Ulasov, S. D. Bader, T. Rajh, M. S. Lesniak, V. Novosad, *Nat. Mater.* **2010**, *9*, 165.
[22] M. Moros, J. Idiago-López, L. Asín, E. Moreno-Antolín, L. Beola, V. Grazú, R. M. Fratila, L. Gutiérrez, J. M. de la Fuente, *Adv. Drug Delivery Rev.* **2019**, *138*, 326.
[23] R. Chen, G. Romero, M. G. Christiansen, A. Mohr, P. Anikeeva, *Science* **2015**, *347*, 1477.
[24] J. Marbaix, N. Mille, J. Carrey, K. Soulantica, B. Chaudret, *Nanoparticles in Catalysis: Advances in Synthesis and Applications*, (Eds.: K. Philippot, A. Roucoux), Wiley, New York **2021**, pp. 307–329.
[25] M. A. Vergés, R. Costo, A. Roca, J. Marco, G. Goya, C. Serna, M. d. P. Morales, *J. Phys. D: Appl. Phys.* **2008**, *41*, 134003.
[26] J. A. Mascorro, G. S. Kirby, *Acta Microscopica* **1992**, *1*, 115.
[27] L. Hou, P. Ning, Y. Feng, Y. Ding, L. Bai, L. Li, H. Yu, X. Meng, *Anal. Chem.* **2018**, *90*, 7122.

[28] T. Kalwarczyk, N. Ziebacz, A. Bielejewska, E. Zaboklicka, K. Koynov, J. Szymanski, A. Wilk, A. Patkowski, J. Gapinski, H.-J. Butt, Robert Hołyst, *Nano Lett.* **2011**, *11*, 2157.
[29] L. Beola, L. Asín, C. Roma-Rodrigues, Y. Fernández-Afonso, R. M. Fratila, D. Serantes, S. Ruta, R. W. Chantrell, A. R. Fernandes, P. V. Baptista, J. M. de la Fuente, V. Grazú, L. Gutiérrez, *ACS Appl. Mater. Interfaces* **2020**, *12*, 43474.
[30] L. Beola, L. Asín, R. M. Fratila, V. Herrero, J. M. De La Fuente, V. Grazú, L. Gutiérrez, *ACS Appl. Mater. Interfaces* **2018**, *10*, 44301.
[31] Y. Fernández-Afonso, L. Asín, L. Beola, M. Moros, J. M. de la Fuente, R. M. Fratila, V. Grazú, L. Gutiérrez, *ACS Appl. Bio Mater.* **2022**, *5*, 1879.
[32] G. Stepien, M. Moros, M. Pérez-Hernández, M. Monge, L. Gutiérrez, R. M. Fratila, M. d. las Heras, S. Menao Guillen, J. J. Puente Lanzarote, C. Solans, J. Pardo, J. M. de la Fuente, *ACS Appl. Mater. Interfaces* **2018**, *10*, 4548.
[33] L. Beola, V. Grazú, Y. Fernández-Afonso, R. M. Fratila, M. de Las Heras, J. M. de la Fuente, L. Gutierrez, L. Asín, *ACS Appl. Mater. Interfaces* **2021**, *13*, 12982.
[34] A. Satoh, *Modeling of magnetic particle suspensions for simulations*, CRC Press, Boca Raton **2017**.
[35] K. Binder, D. W. Heermann, *Monte Carlo simulation in statistical physics*, vol. *8*, Springer, Berlin, Heidelberg **1992**.
[36] S. Suzuki, A. Satoh, M. Futamura, *Mol. Phys.* **2021**, *119*, 1892225.
[37] Z. Zhao, C. Rinaldi, *J. Phys. Chem. C* **2018**, *122*, 21018.
[38] F. Ludwig, H. Remmer, *Phys. Sci. Rev.* **2022**, *7*, 981.
[39] J. P. Segovia-Gutierrez, J. de Vicente, R. Hidalgo-Alvarez, A. M. Puertas, *Soft Matter* **2013**, *9*, 6970.
[40] H. Gavilán, K. Simeonidis, E. Myrovali, E. Mazarío, O. Chubykalo-Fesenko, R. Chantrell, L. Balcells, M. Angelakeris, M. P. Morales, D. Serantes, *Nanoscale* **2021**, *13*, 15631.
[41] A. Satoh, R. W. Chantrell, G. N. Coverdale, *J. Colloid Interface Sci.* **1999**, *209*, 44.
[42] B. Mehdaoui, R. Tan, A. Meffre, J. Carrey, S. Lachaize, B. Chaudret, M. Respaud, *Phys. Rev. B* **2013**, *87*, 174419.
[43] D. P. Valdés, E. Lima, R. D. Zysler, G. F. Goya, E. De Biasi, *Phys. Rev. Appl.* **2021**, *15*, 044005.
[44] D. P. Valdés, E. Lima Jr, R. D. Zysler, E. De Biasi, *Phys. Rev. Appl.* **2020**, *14*, 014023.
[45] E. C. Abenojar, S. Wickramasinghe, J. Bas-Concepcion, A. C. S. Samia, *Prog. Nat. Sci.: Mater. Int.* **2016**, *26*, 440.
[46] L. C. Branquinho, M. S. Carrião, A. S. Costa, N. Zufelato, M. H. Sousa, R. Miotto, R. Ivkov, A. F. Bakuzis, *Sci. Rep.* **2013**, *3*, 1.
[47] S. Ranoo, B. Lahiri, T. Muthukumaran, J. Philip, *Appl. Phys. Lett.* **2019**, *115*, 043102.
[48] A. Y. Zubarev, *Philos. Trans. R. Soc., A* **2019**, *377*, 20180213.
[49] M. Anand, *J. Appl. Phys.* **2020**, *128*, 023903.
[50] S. Ruta, Y. Fernández-Afonso, S. E. Rannala, M. Morales, S. Veintemillas-Verdaguer, C. Jones, L. Gutiérrez, R. W. Chantrell, D. Serantes, *Nanoscale Adv.* **2024**, https://doi.org/10.1039/D4NA00383G.
[51] S. Ruta, R. Chantrell, O. Hovorka, *Sci. Rep.* **2015**, *5*, 9090.
[52] S. Del Sol Fernández, O. F. Odio, P. M. Crespo, E. O. Pérez, G. Salas, L. Gutiérrez, M. D. P. Morales, E. Reguera, *J. Phys. Chem. C* **2022**, *126*, 10110.
[53] M. Moros, B. Hernaez, E. Garet, J. T. Dias, B. Saez, V. Grazu, A. Gonzalez-Fernandez, C. Alonso, J. M. de la Fuente, *ACS Nano* **2012**, *6*, 1565.
[54] R. Hergt, S. Dutz, *J. Magn. Magn. Mater.* **2007**, *311*, 187.
[55] P. M. Pereira, D. Albrecht, S. Culley, C. Jacobs, M. Marsh, J. Mercer, R. Henriques, *Frontiers Immunol.* **2019**, *10*, 675.
[56] J. Klumperman, G. Raposo, *Cold Spring Harbor Perspect. Biol.* **2014**, *6*, a016857.
[57] N. A. Usov, E. M. Gubanova, *Nanomaterials* **2020**, *10*, 1320.
[58] D. Gandia, L. Gandarias, I. Rodrigo, J. Robles-García, R. Das, E. Garaio, J. Á. García, M.-H. Phan, H. Srikanth, I. Orue, J. Alonso, A. Muela, M. L. Fdez-Gubieda, *Small* **2019**, *15*, 1902626.
[59] M. Moros, B. Pelaz, P. López-Larrubia, M. L. García-Martin, V. Grazú, J. M. de La Fuente, *Nanoscale* **2010**, *2*, 1746.
[60] S. A. Shah, D. B. Reeves, R. M. Ferguson, J. B. Weaver, K. M. Krishnan, *Phys. Rev. B* **2015**, *92*, 094438.
[61] H. Mamiya, B. Jeyadevan, *Sci. Rep.* **2011**, *1*, 1.
[62] N. Usov, B. Y. Liubimov, *J. Appl. Phys.* **2012**, *112*, 2.
[63] J. Leliaert, A. Vansteenkiste, A. Coene, L. Dupré, B. Van Waeyenberge, *Med. Biol. Eng. Comput.* **2015**, *53*, 309.
[64] R. Rosensweig, J. Nestor, R. Timmins, *Proc. Symp. AIChE-I.Chem. Eng. Ser.* **1965**, *5*, 104.
[65] N. Metropolis, A. W. Rosenbluth, M. N. Rosenbluth, A. H. Teller, E. Teller, *J. Chem. Phys.* **1953**, *21*, 1087.
[66] A. Satoh, *Introduction to molecular-microsimulation for colloidal dispersions*, Elsevier, Amsterdam **2003**.
[67] M. P. Allen, D. J. Tildesley, *Computer simulation of liquids*, Oxford university press, Oxford **2017**.
[68] A. Satoh, *Introduction to Practice of Molecular Simulation*, Elsevier Science, Amsterdam **2010**.